Professional paper

Informacije MIDEM
Journal of Microelectronics,
Electronic Components and Materials
Vol. 43, No. 4 (2013), 277 – 283

The Copper Losses of Gapped Inductors with Litz-Wire Windings

Alexander Stadler

STS Spezial-Transformatoren Stockach GmbH & Co. KG, Stockach, Germany

Abstract: In this paper, an analytical procedure is presented, how to predict the AC resistance of litz-wire windings considering air gap fringing fields. For this purpose, an equivalent complex permeability model is derived for hexagonally packed wires. It is shown, how the real as well as the imaginary part of the complex permeability can be determined with the copper filling factor as a parameter. An analytical 2D model is deduced to describe the air gap fringing fields of gapped inductors. Accordingly, the proximity losses of the litz-wire winding are determined correctly and the AC resistance of practical inductors can be predicted over a wide frequency range with high accuracy. This offers the opportunity to optimize such components. Finally, the influence of various parameters on the copper losses is investigated and verified by means of experimental data drawn from impedance measurements. The novelty of the approach presented in this paper is given by the fact that an exact 2D analytical solution is conducted to describe the air gap fringing field. Furthermore, the distance between air gap(s) and winding can be considered as a degree of freedom as well as the number of single gaps to realize a distributed air gap.

Keywords: Inductors, air gaps, eddy currents, electromagnetic analysis, analytical models.

Bakrove izgube na tuljavah z režo pri uporabi navitij s pletenico

Izvleček: Članek obravnava analitičen postopek napovedovanja AC upornosti navitja s pletenico. V ta namen je bil razvit model ekvivalentne kompleksne permeabilnosti heksagonalno zavitih žic. Prikazano je, kako se lahko, s pomočjo polnilnega faktorja bakra, določi realen in imaginaren del kompleksne permeabilnosti. Izveden je 2D model opisovanja polja v navitjih z zračno režo. Pravilno so določene izgube bližine v navitju s pletenico. Prav tako je mogoče z visoko natančnostjo določiti AC upornosti v širokem frekvenčnem območju, kar omogoča optimizacijo komponent. V zaključki je, s pomočjo meritev impedance, preučevan vpliv številnih parametrov na izgube v bakru. Novost predstavljene metodologije je natančna 2D analitična rešitev stresanega polja v zračni reži.

Ključne besede: tuljava, zračna reža, vrtinčasti tok, elektromagnetna analiza, analitični model

** Corresponding Author's e-mail: Stadler@STS-Trafo.de*

1 Introduction

High frequency (HF) litz-wire is generally used to avoid strong eddy current losses due to the fringing fields of adjacent air gaps. If the radius *a* of the insulated strands is smaller than the skin depth

$$\delta = \frac{1}{\sqrt{\pi f \sigma \mu_0}} \tag{1}$$

the well known skin effect can be neglected and a homogeneous distribution of the conducted current is expected. Nevertheless, considerably high losses can still be generated due to the fact that all of the strands are influenced by external magnetic fields generated by adjacent strands, windings and air gaps as well (proximity effect).

When designing HF inductors and integrated magnetic components, these effects have to be predicted with high accuracy. Especially air gap fringing fields can lead to much higher losses than expected. As a disadvantage, these losses develop in a small region around the air gap. Due to the poor thermal conductivity of insulated litz-wire, heat cannot be dissipated outside and insulation failures are the consequence.

In recent work (e.g. [1, 2]), eddy current losses of round and rectangular wires have been investigated. These results were extended to bundles of wires [3] and litz-

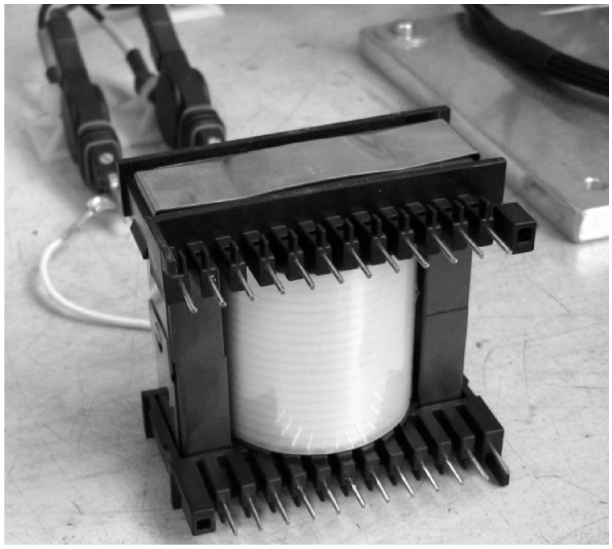

Figure 1: Inductor under test: ETD59/31/22–N87, air gap length l_g=5 mm, number of turns N=72 (litz-wire 7x35x0.1 mm).

wire windings [4, 5]. Nevertheless, numerical simulations as well as analytical solutions (e.g. by the modal decomposition of the boundary value problem) come to their limits when the great number of litz-wire strands has to be taken into account. To provide a solution, equivalent complex permeability models [6 - 9] were derived for the winding area and linked either with FEM simulation or rough (usually 1D) estimations of the penetrating magnetic field.

The novelty of the approach presented in this paper is given by the fact that an exact 2D analytical solution is conducted to describe the air gap fringing field. Furthermore, the distance s between air gap(s) and winding can be considered as a degree of freedom as well as the number of single gaps N_g to realize a distributed air gap (Fig 2).

2 Calculation

2.1 Equivalent Complex Permeability Model

If a round wire is situated in a homogeneous high frequency external magnetic field, eddy currents are generated which again effect the external magnetic field. The shape of this external field part is comparable to a magnetic dipole field. Analogously to the theory of magnetism, a multitude of such dipoles can be expressed by an isotropic complex permeability $\mu = \mu' - \mathrm{j}\mu''$ (Fig. 3). The real part $\mu'(f)$ describes the shielding behavior of the litz-wire region as a function of the frequency f. The imaginary part $\mu''(f)$ is related

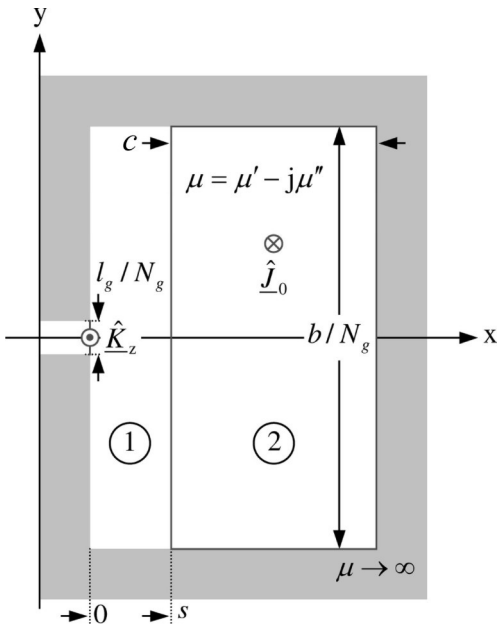

Figure 2: Basic configuration of the winding window (distributed air gap with N_g parts of length l_g/N_g).

to the eddy current losses. To determine $\mu(f)$ of hexagonally packed litz-wire strands, finite element simulation is used.

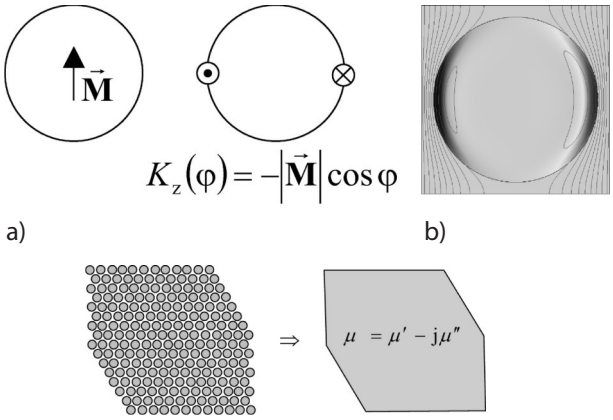

Figure 3: Equivalent current shell of a cylinder with homogeneous magnetization (a), eddy current distribution in a round wire excited by an external magnetic field (b), equivalent complex permeability model for hexagonally packed wires (c).

Fig. 4a shows the FEM simulation of the elementary cell. The picture depicts the absolute value of the electrical current density in a per-cent scale for 50 % copper filling factor and a relation between strand-radius a and skin depth of $a/\delta = 5$.

The real and imaginary parts of the equivalent complex permeability can be determined based on the relations

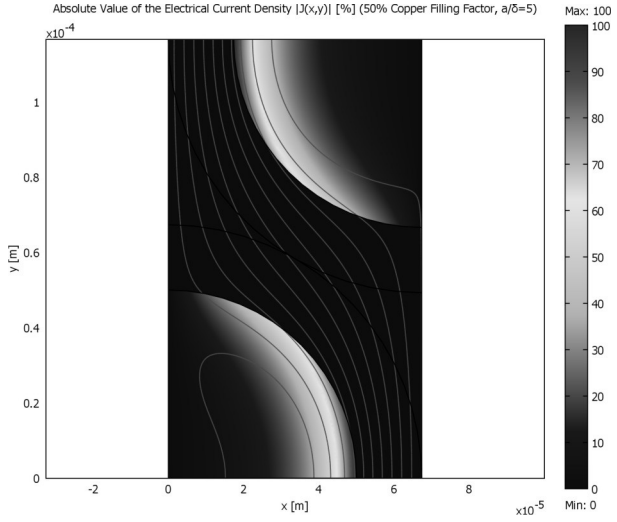

a)

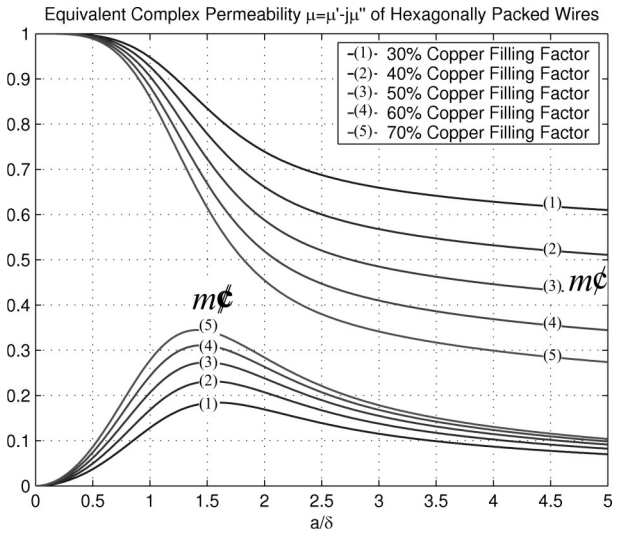

b)

Figure 4: Simulation (a) of the elementary cell of hexagonally packed wires to obtain the equivalent complex permeability $\mu=\mu'-j\mu''$ (b).

$$\mu = \mu' - \mathrm{j}\mu'' = \mu'\left[1 - \mathrm{j}\tan(\varphi_m)\right] \tag{2a}$$

$$\tan(\varphi_m) = \frac{p_m}{2\omega w_m} \tag{2b}$$

$$\mu' = \frac{\overline{B}^2}{4w_m\left[\tan^2(\varphi_m)+1\right]} \tag{2c}$$

where $\tan(\varphi_m)$ denotes the loss tangent, p_m the mean power loss (per volume) and w_m the mean stored magnetic energy (per volume). In Fig. 4b the results are presented with different values of the copper filling factor as a parameter.

2.1 Analytical Calculation of the Winding Proximity Losses

With the equivalent complex permeability presented above, the calculation of the winding proximity losses can be referred to a magnetostatic problem. The basic configuration is depicted by Fig. 2. Therein, *b* denotes the width of the core's winding window and *c* the thickness of the litz-wire winding.

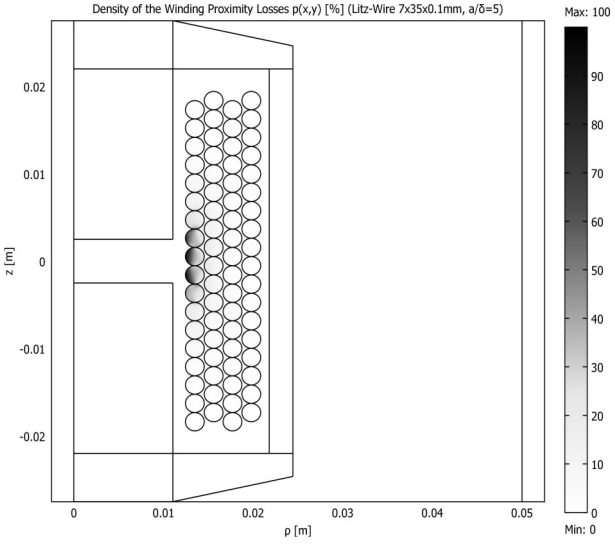

a)

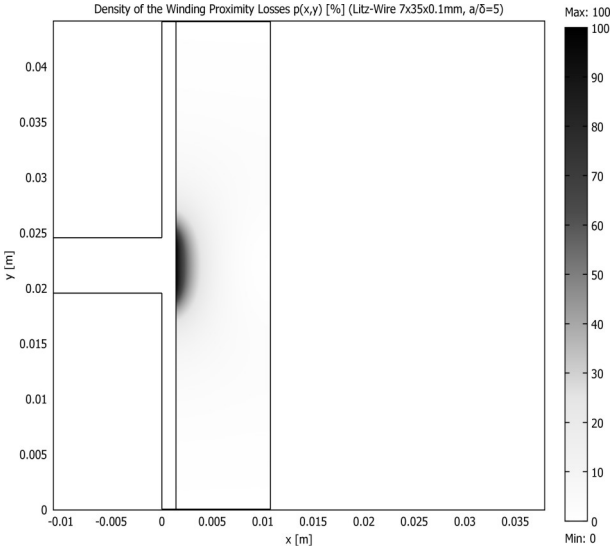

b)

Figure 5: Simulated proximity loss density of the litz-wire region due to the air gap fringing field for complex (a) as well as simplified (b) geometry ($a/\delta = 5$).

To begin with, it is verified, if the geometry of the winding window can be restricted to the relatively simple configuration shown in Fig. 2 with acceptable error. Therefore, FEM simulations are conducted to investigate the influence of the underlying geometry on the

calculated AC winding resistance. Fig. 5 depicts both alternatives. In Fig. 5a the complex axially symmetric model with distinct litz-wire windings is shown (each with copper filling factor 0.6). In Fig. 5b the plane 2D restricted model is figured out. Therein, the spacing between the round windings is considered by the total copper filling factor (here 0.38) of the winding area.

The color bar in Fig. 5 is related to the simulated proximity loss density of the litz-wire region (per cent scale). Using FEM, the total proximity losses can be determined via integration. By superposition of DC (RMS), skin and proximity losses, the AC resistance is calculated and illustrated by Fig. 6a. In Fig. 6b the relation R_{AC}/R_{DC} is shown. From these results, it can be seen that the basic geometry can be restricted according Fig. 2 with acceptable error.

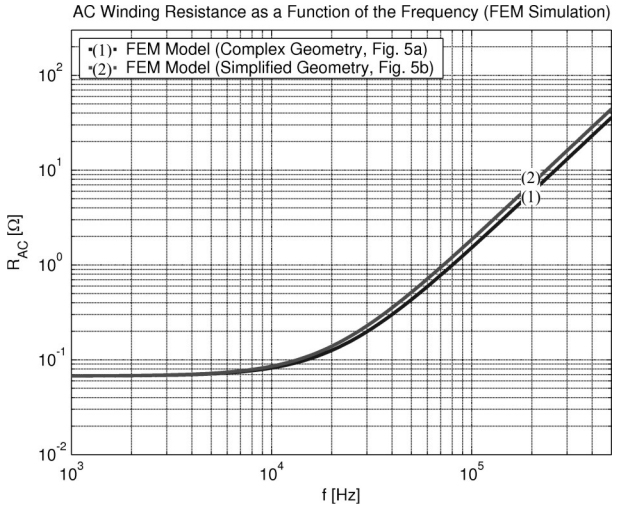

a)

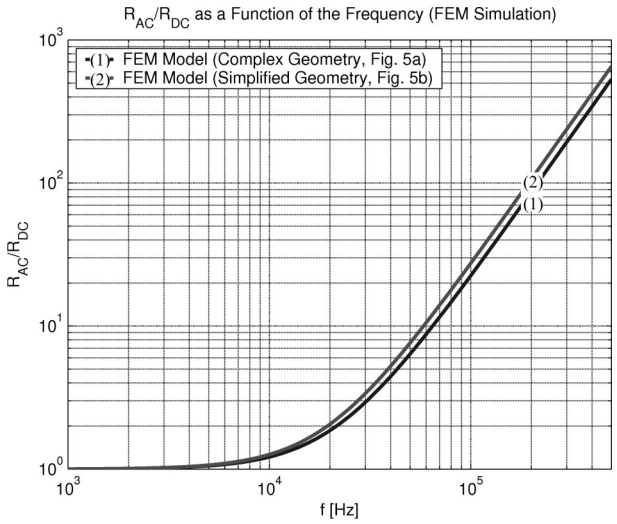

b)

Figure 6: AC resistance (a) and relation R_{AC}/R_{DC} (b) for complex (Fig. 5a) and simplified geometry (Fig. 5b).

The two-dimensional solution is based on the (complex) magnetic vector-potential $\underline{\hat{\mathbf{A}}} = \vec{\mathbf{e}}_z \underline{\hat{A}}_z(\mathrm{x},\mathrm{y})$, which has to fulfill the vectorial partial differential equation

$$\nabla \times \left(\nabla \times \underline{\hat{\mathbf{A}}} \right) = \begin{cases} \vec{\mathbf{0}} & \text{region 1} \\ & \text{in} \\ -\mu \underline{\hat{J}}_0 \, \vec{\mathbf{e}}_z & \text{region 2} \end{cases} . \quad (3)$$

After R-separation [10, 11] of the according scalar differential equation and restriction by the different boundary conditions, for region 1 and 2 in Fig. 2, the two solutions

$$\underline{\hat{A}}_{z1}(\mathrm{x},\mathrm{y}) = \underline{\hat{A}}_0 + \underline{\hat{B}}_0 \mathrm{x} + + \sum_{n=1}^{+\infty} \left[\underline{\hat{A}}_n \frac{\cosh(\lambda_n \mathrm{x})}{\cosh(\lambda_n s)} + \underline{\hat{B}}_n \frac{\sinh(\lambda_n \mathrm{x})}{\sinh(\lambda_n s)} \right] \cos(\lambda_n \mathrm{y}) \quad (4a)$$

$$\underline{\hat{A}}_{z2}(\mathrm{x},\mathrm{y}) = \frac{1}{2} \mu \underline{\hat{J}}_0 \left[\mathrm{x} - (s+c) \right]^2 + + \sum_{n=1}^{+\infty} \underline{\hat{E}}_n \frac{\cosh\left\{ \lambda_n \left[\mathrm{x} - (s+c) \right] \right\}}{\cosh\left\{ \lambda_n \left[s - (s+c) \right] \right\}} \cos(\lambda_n \mathrm{y}) \quad (4b)$$

are found. With the eigenvalues $\lambda_n = 2\pi \, n \, N_g / b$ and the parameters

$$\underline{\hat{B}}_0 = -\mu_0 \underline{\hat{J}}_0 \, c$$

$$\underline{\hat{A}}_0 = \frac{1}{2} \mu \underline{\hat{J}}_0 c^2 - \underline{\hat{B}}_0 s$$

$$\underline{\hat{B}}_n = -\frac{\mu_0}{\lambda_n} \underline{\hat{J}}_0 \frac{bc}{l_g} \frac{2}{\pi n} \sin\left(\frac{\pi n l_g}{b} \right) \sinh(\lambda_n s)$$

$$\underline{\hat{E}}_n = \underline{\hat{B}}_n \left[1 - \tanh^{-2}(\lambda_n s) \right] \left(1 + \frac{\mu_0}{\mu} \frac{\tanh\{\lambda_n c\}}{\tanh(\lambda_n s)} \right)^{-1}$$

$$\underline{\hat{A}}_n = \underline{\hat{E}}_n - \underline{\hat{B}}_n$$

the proximity losses of the winding area 2 in Fig. 2 can be calculated using Poynting's theorem.

3 Results

Accordingly, the winding proximity losses per length *l* are given by

$$\frac{\overline{P}_v^{(Prox)}}{l} = \frac{N_g \omega}{2\mu_0} \mathrm{Im} \left\{ \frac{b}{N_g} \underline{\hat{A}}_0 \underline{\hat{B}}_0^{\,*} + \sum_{n=1}^{+\infty} \pi \, n \frac{\underline{\hat{A}}_n}{\cosh(\lambda_n s)} \frac{\underline{\hat{B}}_n^{\,*}}{\sinh(\lambda_n s)} \right\} \quad (5)$$

3.1 Calculation of the Total Copper Losses

If the winding with current $i(t) = \hat{i}\cos(\omega t)$ consists of *N* turns of litz-wire, each with *M* strands of diameter *d*, the DC (RMS) losses can be described by

$$\frac{\overline{P}_v^{(RMS)}}{l} = \frac{1}{2}\frac{N}{\sigma M \pi\left(\frac{d}{2}\right)^2}\hat{i}^2 \tag{6}$$

The copper losses due to the skin effect now are directly calculated from the RMS losses:

$$\frac{\overline{P}_v^{(Skin)}}{l} = \left[\frac{d}{4\delta}\mathrm{Re}\left\{(1+\mathrm{j})\frac{\mathrm{I}_0\left[(1+\mathrm{j})\frac{d}{2\delta}\right]}{\mathrm{I}_1\left[(1+\mathrm{j})\frac{d}{2\delta}\right]}\right\} - 1\right]\frac{\overline{P}_v^{(RMS)}}{l} \tag{7}$$

The total copper losses are finally given by the superposition of all loss mechanisms:

$$\frac{\overline{P}_v}{l} = \frac{\overline{P}_v^{(RMS)}}{l} + \frac{\overline{P}_v^{(Skin)}}{l} + \frac{\overline{P}_v^{(Prox)}}{l} \tag{8}$$

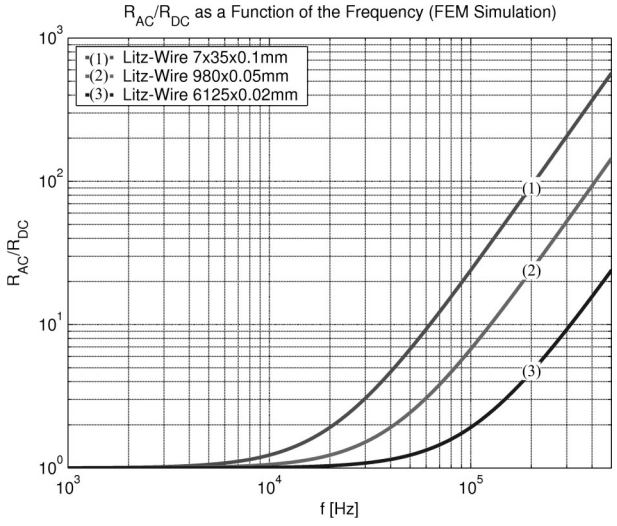

Figure 7: Relation R_{AC}/R_{DC} for different types of litz-wire.

Fig. 7 depicts the relation $\overline{P}_v / \overline{P}_v^{(RMS)} = R_{AC}/R_{DC}$ for different types of litz-wire (R_{DC} is kept constant in all cases). It can be noticed that the AC resistances are increasing much earlier than estimated by the skin depth (1). E.g. for 0.1 mm strand-diameter, we reach $a/\delta \approx 1$ at ~1.75 MHz – in contrast the AC resistance starts to increase around 10 kHz(!).

This is a direct consequence of the fact that proximity losses are predominant here. The diagram shows that frequency could be around five times higher at constant copper losses using 0.02 mm strand diameter instead of 0.1 mm (sinusoidal current).

4 Inductor Optimization: Minimization of Copper Losses

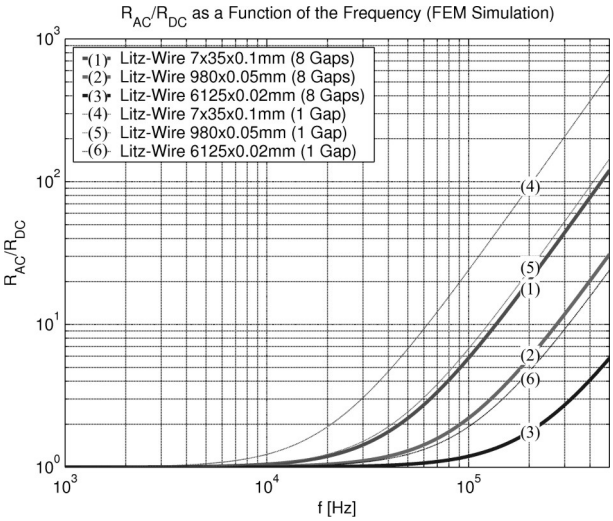

a)

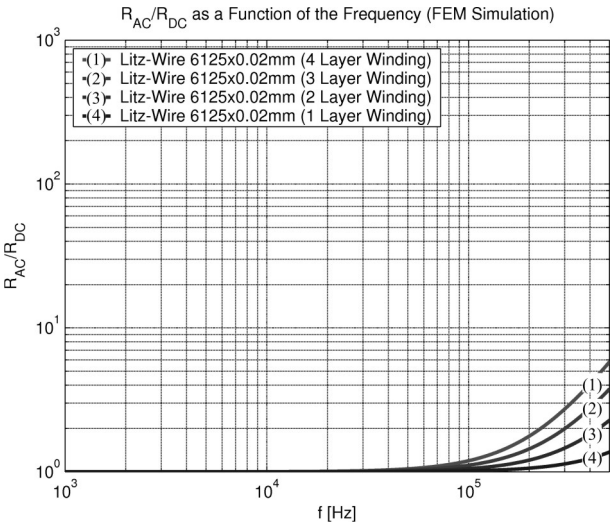

b)

Figure 8:. Relation R_{AC}/R_{DC} (a) for different types of litz-wire and a distributed air gap of 8 single gaps (thick lines), R_{AC}/R_{DC} for different numbers of layers (b).

To reduce the copper losses, the choice of thinner strand diameters may not be the most cost effective way. In many cases, the realization of a distributed air gap could be an alternative [12]. In Fig. 8a the original 5 mm central air gap is split into 8 single air gaps, each of length 0.385 mm. To give a fair comparison, the inductance of the choke is kept constant. It is found that

the advantage of the distributed air gap here is close to the gain of choosing the next thinner strand diameter (thin lines). The influence of the number of layers on the relation R_{AC}/R_{DC} is presented in Fig. 8b. Using a one-layer-winding (see Fig. 11) and the suggested litz-wire 6125x0.02 mm, a 500 kHz resonant power inductor can be realized with copper losses comparable to the DC case.

a) b)

Figure 9: High frequency equivalent circuit model (a) of the inductor, Wayne-Kerr 3260-B impedance analyzer (b) used for measurements.

5 Experimental Verification

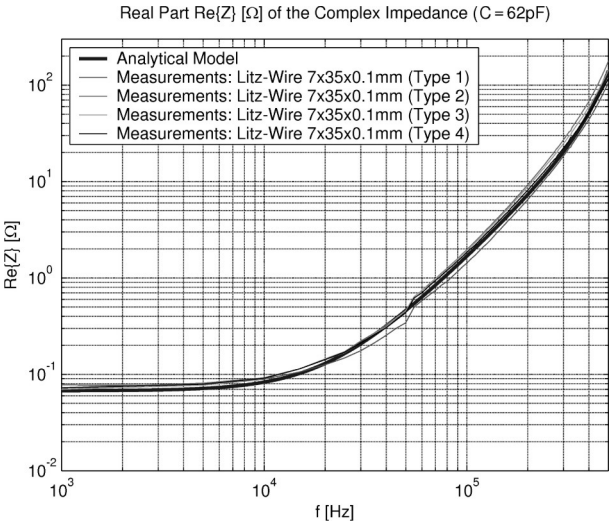

Figure 10: Comparison between simulated and measured results for different types of 7x35x0.1 mm litz-wire (parameter: twist pitch length).

In Fig. 10 the simulation results are compared with measured data. Four different types of litz-wire are used for measurements – each with different twist pitch length. To describe the parasitic effects of the inductor, a constant parallel capacitance C ≈ 62 pF is assumed (see equivalent circuit model in Fig. 9a). The Wayne-Kerr 3260-B impedance analyzer which was used for measurements is shown in Fig. 9b. The (measured) series resistance R_S and series inductance L_S are finally given by the expressions

$$R_s = \mathrm{Re}\{\underline{Z}\} = \frac{R}{\left(1-\omega^2 LC\right)^2 + \left(\omega RC\right)^2} \tag{9a}$$

$$L_s = \omega^{-1} \cdot \mathrm{Im}\{\underline{Z}\} = \frac{L - \omega^2 L^2 C - R^2 C}{\left(1-\omega^2 LC\right)^2 + \left(\omega RC\right)^2} \tag{9b}$$

Fig. 10 illustrates the high accuracy of the model. It is found that the proximity losses are more or less independent from the twist pitch length of the litz-wire. Consequently, the model becomes more general and the only relevant parameters to describe an arbitrary litz-wire are the strand diameter and the copper filling factor.

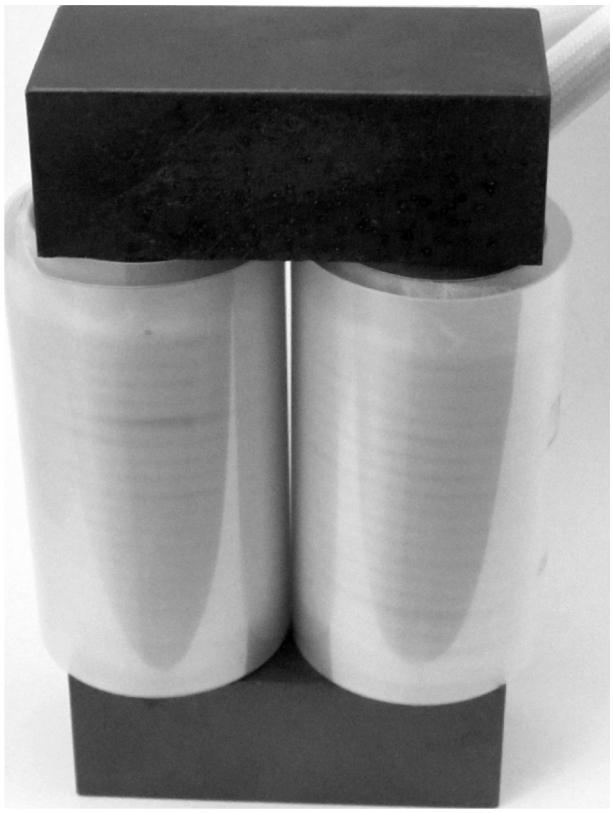

Figure 11: Optimized inductor with distributed air gap and one-layer-winding

6 Conclusion

Promising experimental results show that the litz-wire model allows a precise prediction of the winding AC resistance even if strong air gap fringing fields penetrate the winding. The strand-diameter and the copper filling factor are identified as the only necessary parameters to describe practical litz-wires. This offers the opportunity to optimize these components. If the winding window and the copper cross section are fixed, the strand diameter and the number of gaps (if a distributed air gap can be realized) remain as degrees of freedom.

Otherwise, also the number of layers can be taken into account. In most cases, the main goal of the optimization process is to minimize the AC resistance for a given amount of copper. To exemplify the major dependencies, various parameter studies are shown in the paper based on the example inductor and different types of litz-wire.

References

1. X. Nan and C. R. Sullivan, "An improved calculation of proximity-effect loss in high-frequency windings of round conductors," IEEE Power Electronics Specialists Conference PESC, pp. 853-860, June 2003.
2. C. Larouci, J. P. Keradec, J. P. Ferrieux, L. Gerbaud, and J. Roudet, "Copper losses of flyback transformer: Search for analytical expressions," IEEE Transactions on Magnetics, vol. 39, no. 3, pp. 1745-1748, 2003.
3. J. Gyselinck and P. Dular, "Frequency-domain homogenization of bundles of wires in 2-d magnetodynamic FE calculations," IEEE Transactions on Magnetics, vol. 41, no. 5, pp. 1416-1419, 2005.
4. F. Tourkhani and P. Viarouge, "Accurate analytical model of winding losses in round Litz wire windings," IEEE Transactions on Magnetics, vol. 37, no. 2, pp. 538-543, 2001.
5. J. A. Ferreira, "Analytical computation of AC resistance of round and rectangular litz wire windings," IEE Proceedings-B – Electric Power Applications, vol. 139, no. 1, pp. 21-25, Jan. 1992.
6. O. Moreau, L. Popiel, and J. Pages, "Proximity losses computation with a 2D complex permeability modelling," IEEE Transactions on Magnetics, vol. 34, no. 5, pp. 3616-3619, 1998.
7. X. Nan and C. R. Sullivan, "An equivalent complex permeability model for litz-wire windings," IEEE IAS, vol. 40, no. 3, pp. 2229-2235, 2005.
8. H. Roßmanith, M. Döbrönti, M. Albach, and D. Exner, "Measurement and characterization of high frequency losses in nonideal litz wires," IEEE Transactions on Power Electronics, vol. 26, no. 11, pp. 3386-3394, Nov. 2011.
9. H. Roßmanith, M. Albach, J. Patz, and A. Stadler, "Improved characterization of the magnetic properties of hexagonally packed wires," 14th European Conference on Power Electronics and Applications EPE, Aug. 2011.
10. J. D, Jackson, Classical Electrodynamics, 2nd ed., John Wiley & Sons, New York, 1975.
11. W. R. Smythe, Static and Dynamic Electricity, 3rd ed., McGraw-Hill, New York, 1968.
12. A. Rahimi-Kian et al., "Minimum loss design of a 100kHz inductor with litz wire," 32nd IEEE IAS Conference, vol. 2, pp. 1414-1420, 1997.

Arrived: 18. 09. 2013
Accepted: 27 .11. 2013